Magnetic-Field-Induced Isotropic-Nematic Phase Transition in a Colloidal Suspension

Jianxin Tang and Seth Fraden
Martin Fisher School of Physics, Brandeis University, Waltham, Massachusetts 02254
(Received 11 August 1993)

Evidence of a magnetic-field-induced isotropic-nematic phase transition is presented for a colloidal suspension of monodisperse *fd* virus, a semiflexible particle with a length-to-diameter ratio of ~ 140. The dynamics of the phase transition are slow enough to study the unstable portion of the phase diagram and the subsequent phase separation.

PACS numbers: 64.70.Md, 61.25.Hq, 61.30.Gd

We study a magnetic-field-induced isotropic-nematic phase transition in aqueous colloidal suspensions of the bacteriophage *fd*, and its close relative $m13$, which are long, semiflexible filamentous viruses [1]. For low concentrations of *fd* the angular distribution function $[f(\theta)]$, which characterizes the probability of finding a particle with its long axis pointing in a particular direction, is uniform and the phase is optically isotropic. As the concentration is increased to a volume fraction of (1–2)% the sample undergoes a spontaneous first order phase transition to a chiral nematic phase [2] and the angular distribution becomes anisotropic.

It has long been predicted that an external field, which orients the particles long axis along the field, will induce a first order phase transition if the isotropic phase (I) is thermodynamically near the nematic phase (N) in the absence of the field [3,4]. Here, we present the first experimental evidence of a magnetic-field-induced I-N phase transition in any liquid crystal. An unusual feature, particular to lyotropics, is that the phase transition involves two order parameters, one characterizing angular order and the other the particle concentration in the coexisting phases. We determine the equilibrium concentration–magnetic-field phase behavior in suspensions of *fd* and $m13$ by measuring the field-induced birefringence and through direct observation of the phase separation in a microscope. We observe that the time constants for the evolution of the two order parameters are very different. As a consequence, we are able to follow the dynamics of phase separation from the unstable portion of phase diagram through the spinodal decomposition. This is exceptional because usually a system stays in the unstable phase for too short a time to observe experimentally.

Previously thermotropic liquid crystals have been used to study field-induced transitions [5]. Because of the small size of the molecules, magnetic fields of order 1 MG are needed to observe the critical point [3], which is well above current obtainable field strengths. Only recently has the phase transition been observed using short bursts of high voltage ac fields [6].

The viruses *fd* and $m13$ are 900 nm in length (L), 6.5 nm in diameter (D) [1], and have a persistence length (P) of 2200 nm [7]. They are of 1.6×10^7 g/mole molecular weight and at pH 7–8 are negatively charged with a linear charge density of $10e$/nm [8]. In all our studies, the viruses were suspended in 10mM potassium phosphate buffer at pH 7.2, which has an ionic strength of 23mM. The concentrations of the coexisting isotropic c_i and chiral nematic c_a phases of freshly prepared *fd* were $c_i = 12.6$ mg/ml and $c_a = 14.0$ mg/ml. We observed a shift of c_i and c_a to higher values with time amounting to a 2% increase in each after three weeks. The $m13$ sample discussed in this paper had $c_i = 15.6$ mg/ml. The physical origin of this time dependence is unknown. Experimental data are compared only when taken within 24 h of each other. The magnetic birefringence experiments were performed at the Francis Bitter National Magnet Laboratory (FBNML) in a 20 T magnet equipped with a temperature stabilized holder, which was regulated at 22.0 °C. Sample cells for all experiments had a 3 mm path length and were illuminated with a 1 mm diam HeNe laser (633 nm) for birefringence measurements or white light for microscopy.

To search for a field-induced transition we built a 100× polarizing microscope to fit in a 20 T magnet and examined visually the isotropic samples in coexistence with the chiral nematic. Initially when the field was swept from zero to 14 T in 30 sec, the intensity increased from dark to bright white, then uniform interference colors swept through the sample. After 1 min small domains of several microns in size appeared uniformly throughout the sample forming an amorphous network and, after 30 min, the droplets coarsened to order 20 μm. When the field was rapidly reduced to zero, the field-induced network vanished rapidly. The direct observation of droplet formation demonstrates that a first order phase transition has occurred, and the asymmetry in the times for buildup and decay of the droplets indicate that the dynamics of this process are very interesting. We set out to study the dynamics in detail by measuring the specific magnetic-field-induced birefringence $\Delta n/c$.

In our experiments $\Delta n/c$ was linear in field energy for small fields and for all concentrations as observed previously [9]. However, we observed a large nonlinear increase in $\Delta n/c$ at high fields for concentrations in a narrow range of the I-N transition. Deviations

0031-9007/93/71(21)/3509(4)$06.00

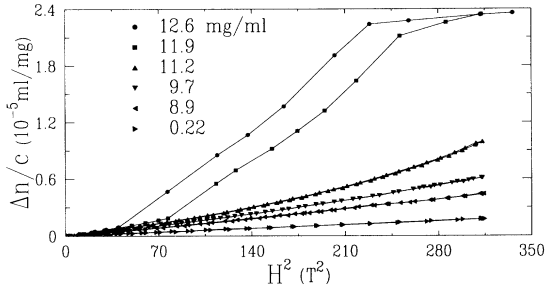

FIG. 1. The specific magnetic-field-induced birefringence ($\Delta n/c$) as a function of field squared (H^2), for *fd* concentrations spanning the entire isotropic range at zero field. Data were taken after the sample was equilibrated in the field, and the entire set was obtained in a day.

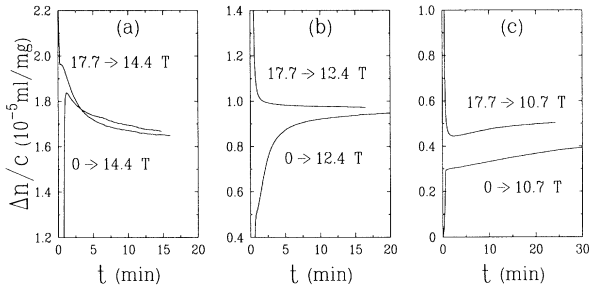

FIG. 3. Time dependence (t) of the specific field-induced birefringence ($\Delta n/c$) for *fd*. (a)–(c) A field jump from zero and a field quench from 17.7 T to the final values of 10.7, 12.4, and 14.4 T, respectively.

from linear response were not observed previously [9] because the maximum magnetic field was 1 T, while at the FBNML we used fields up to 20 T, resulting in field energies a factor of 400 times greater. The nonlinear increase, shown in Fig. 1 for freshly prepared *fd*, is indicative of field-induced order, as opposed to a linear response where the birefringence is due to the aligning of the existing correlation volumes along the field direction. At the highest fields, and for the highest concentrations one sees evidence of saturation of the birefringence, indicating the complete formation of a field-induced nematic phase. Figure 1 demonstrates that the minimum concentration for which a field-induced transition occurs is within (5–10)% of c_i.

The dynamics of the induced birefringence is very rich. Beginning with equilibrated isotropic samples in coexistence with the chiral nematic at zero field we rapidly increased the field to a "low" value [10.7 T for *fd*, Fig. 3(c), 12.4 T for $m13$, Fig. 2] and observed a monotonic increase in the birefringence whose time response has a fast and slow component. If instead the field is increased to "high" field (greater than 16.8 T for $m13$, Figs. 2 and 4) where the saturation regime begins, the alignment approaches a steady state monotonically with only the fast component in the response. In contrast, for intermediate values of the field, the birefringence increases to a maximum within a minute after the field is applied and then slowly decays to a steady-state value. The magnitude of the overshoot is a function of the field and is illustrated in Fig. 2 for $m13$.

We also studied the dynamics of field quenches for the *fd* sample of $c = 12.6$ mg/ml taken 3 weeks after the data in Fig 1. Because of the upwards shift of the coexistence concentrations with time, this sample behaves similarly to the sample of 11.9 mg/ml in Fig. 1. In a quench we equilibrate the sample at a high field (17.7 T) and then rapidly lower the field. When we quench to a low field (10.7 T) we observe a rapid decrease of the birefringence to a minimum, followed by a slow increase to a steady state value greater than that obtained with a field jump from 0 to 10.7 T, indicating hysterisis [Fig 3(c)]. After reequilibration at 17.7 T and then quenching

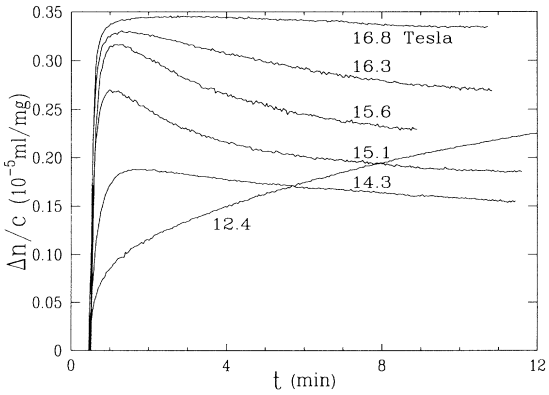

FIG. 2. Time dependence (t) of the specific field-induced birefringence ($\Delta n/c$) following an increase in field from zero to the field indicated in tesla for a coexisting isotropic sample of $m13$, $c_i = 15.6$ mg/ml. Only a portion of the curve is shown and each curve has been offset by an arbitrary amount for display purposes.

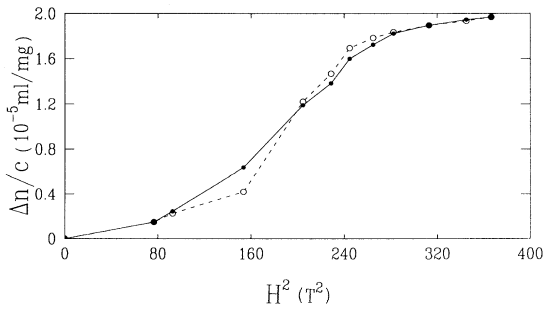

FIG. 4. The specific magnetic-field-induced birefringence ($\Delta n/c$) as a function of field squared (H^2) for the $m13$ sample of Fig. 2. Curve (○): maximum values of $\Delta n/c$ if an overshoot occurs or the value of the birefringence 1 min after the field achieved its set value. Curve (●): long time values.

to 14.4 T, we now find that the initial undershoot of the birefringence no longer occurs. Instead, the birefringence decreases monotonically to the same value obtained with a field jump from 0 to 14.4 T [Fig. 3(a)]. Finally, after a field quench from 17.7 to 12.4 T the birefringence decreases monotonically and approaches the value equal to the birefringence resulting from a field jump from 0 to 12.4 T [Fig. 3(b)]. In summary, we find that whenever an overshoot in birefringence occurs with a field jump from zero to a certain intermediate field, we never observe an undershoot with a quench from high field to the same intermediate field. Likewise whenever a quench from high to low field produces an undershoot in the birefringence, a jump from zero field to the same low field does not produce an overshoot.

In Fig. 4 we plot the maximum value of the birefringence for $m13$ in the case of an overshoot of birefringence (Fig. 2) or the birefringence 1 min after the field reaches its new value if no overshoot is observed as a function of field energy. This time is long enough for the fast component to have relaxed, but is too short for the steady state value to be obtained, as is evidenced in Fig. 2. This curve has a sigmoidal character. In the same figure we also plot the long time birefringence as a function of field energy. This curve increases in an approximately linear fashion and eventually saturates at high fields. The data are derived from Fig. 2.

The phase diagram as a function of field has been calculated by Khoklov and Semenov [4] using the Onsager variational trial function [10] for the two cases of rigid ($P = \infty, L \gg D$) and flexible ($L \gg P \gg D$) neutral particles. They find the same qualitative phase behavior for these two cases. The model of charged polymers with intermediate flexibility is not yet solved. Since we are seeking a qualitative understanding of the birefringence data, we compare our results of the field experiments with the theoretical predictions of the Onsager model for rigid rods [10], which we solve numerically using an iterative solution of the angular distribution function. This calculation was done previously by Lee [11] for the case of elongational flow, a potential with the same symmetry as the magnetic field.

In Fig. 5 the calculated field-concentration phase diagram is shown. The critical point occurs at a ratio of the field energy to thermal energy ($\mathcal{H} = \Delta\chi H^2/kT$) of $\mathcal{H}_c = 1.02$. The concentration is expressed in dimensionless units, $q = \pi DL^2 n/4$, with n the particle number density [4,10,11]. At a finite value of the field the two coexisting phases are a weakly aligned phase with a strongly aligned phase [3,4]. The strongly aligned phase is a nematic since any chirality is unwound by the large fields. The lowest concentration for which a field-induced phase transition will occur is $q = 3.12$ and the coexisting concentrations at zero field are $q_i = 3.29$ and $q_a = 4.19$. In Fig. 6 the order parameter $S = \int f(\theta) P_2(\theta) d\Omega$, with $P_2(\theta)$ the second Legendre polynomial, is shown as a function of $\mathcal{H}$ for the coexisting phases. S is directly proportional to the experimentally measured specific field-induced birefringence, $\Delta n/c$. The highest concentration is $q_i = 3.29$ and two curves are shown for its field-induced order parameter in the coexisting region of the S-$\mathcal{H}$ phase diagram in Fig. 6. The sigmoidal curve (dashed) is calculated assuming no phase separation occurs, i.e., that the concentration stays constant at $q_i = 3.29$ as the field is increased (the vertical line in Fig. 5). In contrast, the linear curve (solid line) in Fig. 6, assumes complete phase separation occurs and the relative amount of each phase is calculated using the lever rule applied along the $q_i = 3.29$ line in the $\mathcal{H}$-q plane. Then the order parameter is calculated as the weighted sum of the coexisting order parameters shown in Fig. 6. This would be proportional to the observed birefringence if the measurement averaged over the two phases. The second curve in Figs. 5 and 6 corresponds to a concentration of $q_c = 3.2$, the

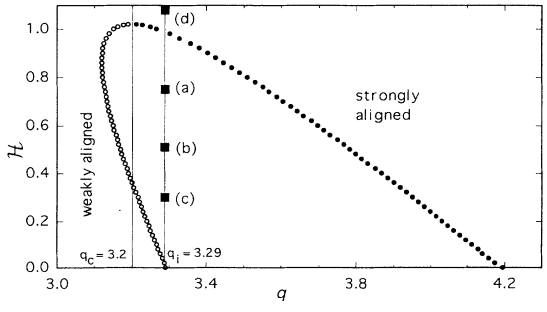

FIG. 5. The calculated field-energy–concentration phase diagram is shown as a function of the dimensionless parameters $\mathcal{H} = \Delta\chi H^2/kT$ vs $q = \pi DL^2 n/4$. The coexistence curve separates weakly (○) from strongly (●) aligned nematic phases.

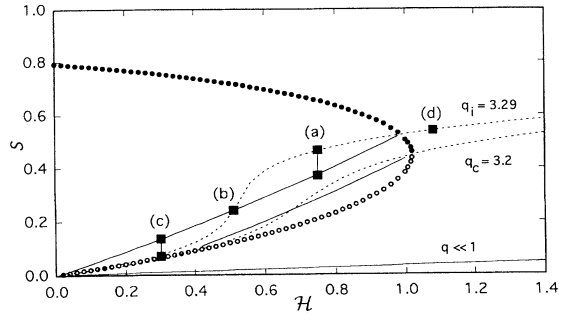

FIG. 6. The order parameter (S) and field energy $\mathcal{H} = \Delta\chi H^2/kT$ phase diagram. The coexistence curve separates weakly (○) from strongly (●) aligned nematic phases. The order parameter for the coexisting and critical concentrations, q_i and q_c, is indicated. Each concentration has two curves—the sigmoidal curve (dotted line) assumes no phase separation occurs along the corresponding constant concentration paths in Fig. 5, while the solid line is the average S assuming complete phase separation.

critical concentration.

The behavior of $\Delta n/c$ as a function of time, including the undershoots and overshoots can be understood with the aid of Figs. 5 and 6. In Fig. 5 four points (a)–(d), are indicated along the $q_i = 3.29$ line and correspond to the labeled points indicated in Fig. 6. Consider an isotropic sample in coexistence with the ordered phase at zero field ($\mathcal{H} = 0, q_i = 3.29$, Fig. 5). Then, suddenly increase the field to $\mathcal{H} = 0.75$ to point (a) in Fig. 5. The sample finds itself in the coexistence region of the phase diagram and decomposes into the weakly and strongly ordered phases. In the S-$\mathcal{H}$ plane of Fig. 6 the order parameter jumps from zero to 0.47, which is on the sigmoidal portion of the q_i line and is above the equilibrium value. Subsequently, S decays to the equilibrium value, i.e., an overshoot of the order parameter occurs. Now equilibrate the same sample at a high field, point (d) in Fig. 5, which is greater than the critical point and rapidly quench the field to point (a). The sample again finds itself at point (a) along the sigmoidal portion of the q_i line in Fig. 6, but this time decreases monotonically to the equilibrium value (no undershoot). The experimental situation is shown in Fig. 3(a). The undershoot case is demonstrated by first equilibrating the sample at zero field and then rapidly increasing the field to $\mathcal{H} = 0.3$ [point (c) in Fig. 5]. The sigmoidal portion of the q_i line in Fig. 6 at point (c) has an order parameter less then the equilibrium value; thus no overshoot occurs. However, when the sample is equilibrated at point (d) in Fig. 5 and then quenched to point (c), an undershoot in birefringence occurs. This compares well with the data shown in Fig. 3(c). The observation of hysterisis in Fig. 3(c) indicates it lies below the spinodal line. Since point (b) in Fig. 5 is near the crossover of the unstable and equilibrium values of S, no overshoot or undershoot in S is observed. This is similar to the experimental case of Fig. 3(b). This model also predicts that there will be a range of fields for which only overshoot occurs and a complementary range of fields where only undershoots are possible. In Fig. 6 the crossover between undershoot and overshoot behavior occurs at $\mathcal{H} = 0.5$ for q_i. The corresponding experimental data are presented in Figs. 2–4.

Our explanation of the experimental data shown in Figs. 1–4 relies on two assumptions. First, the time constant for realignment of the particles in response to a field jump to the unstable portion of the phase diagram occurs much faster than the subsequent phase separation, and, second, the sample volume from which the birefringence is measured contains enough two-phase domains to effectively average the birefringence of the two phases. While our microscopic observations support the assumption that the droplets are small, we can only speculate that the droplets that form 1 min after a field jump are not yet at their final concentration (and order parameter), which is obtained about 30 min later. The phase separation process involves mass transport of particles, which may be much slower than their reorientation from the isotropic to unstable portion of the phase diagram. The sudden disappearance of the network after removing the field from a two-phase sample that has taken a long time to form in a field is an additional interesting kinetic feature, and also requires further theoretical and experimental investigation.

The range of concentrations over which the field induced transition can occur is predicted to be about 5% of c_i for both the rigid (Fig. 5) and flexible models [4], in accordance with our observations (Fig. 1). Finally, we can estimate the critical field, which as seen in Fig. 6 is expected to be near the field for which saturation in the birefringence occurs. We observe this field to be 17 T (Fig. 1). Using the literature value of $\Delta\chi = 7 \times 10^{-24} J/T^2$ [12] we find $\mathcal{H} = 0.5$. This is less than predicted for rigid rods but close to the critical field predicted for persistent polymers [4].

We thank E. Bullet, L. Makowski, M. Cahoon, and Z. Dogic for assistance in the preparation of virus. We thank G. Maret and S. F. Schulz for conveying their unpublished magnetic birefringence data on *fd* to us, and T. J. Sluckin, G. J. Vroege, H. N. W. Lekkerkerker, and R. B. Meyer for many stimulating discussions. We acknowledge support from NSF DMR 4-59850.

[1] S. Bhattacharjee, M.J. Glucksman, and L. Makowski, Biophys. J. **61**, 725 (1992).
[2] J. Lapointe and D.A. Marvin, Mol. Cryst. Liq. Cryst. **19**, 269 (1973).
[3] J. Hanus, Phys. Rev. **178**, 420 (1969); C. Fan and M. Stephen, Phys. Rev. Lett. **25**, 500 (1970); P.J. Wojtowicz and P. Sheng, Phys. Lett. **48A**, 235 (1974); R.M. Hornreich, Phys. Lett. **109A**, 232 (1985).
[4] A.R. Khokhlov and A.N. Semenov, Macromolecules **15**, 1272 (1982).
[5] A.J. Nicastro and P.H. Keyes, Phys. Rev. A **30**, 3156 (1984).
[6] I. Lelidis and G. Durand, Phys. Rev. E (to be published).
[7] T. Maeda and S. Fujime, Macromolecules **18**, 2430 (1985); E. Loh, E. Ralston, and V.N. Schumaker, Biopolymers **18**, 2549 (1979); E. Loh, *ibid.* **18**, 2569 (1979); K. Beck and R.M. Duenki, J. Struct. Biol. **105**, 22 (1990); L. Song, U-S. Kim, J. Wilcoxon, and J.M. Schurr, Biopolymers **31**, 547 (1991).
[8] K. Zimmermann, J. Hagedorn, C.C. Heuck, M. Hinrichsen and J. Ludwig, J. Biol. Chem. **261**, 1653 (1986).
[9] H. Nakamura and K. Okano, Phys. Rev. Lett. **50**, 186 (1983).
[10] L. Onsager, Ann. N.Y. Acad. Sci. **51**, 627 (1949).
[11] S-D. Lee, J. Chem. Phys. **86**, 6567 (1987).
[12] J. Torbet and G. Maret, Biopolymers **20**, 2657 (1981).